

# Multiobjective Path Planning for Autonomous Robotic Percutaneous Nephrolithotomy via Discrete B-spline Interpolation\*

Olivia Wilz<sup>1</sup>, Ben Sainsbury<sup>2</sup>, and Carlos Rossa<sup>1</sup>

**Abstract**—Percutaneous nephrolithotomy is the leading treatment for large or irregularly shaped kidney stones. Nevertheless, gaining access to the kidney remains a challenging component of the procedure with a steep learning curve. As a result, the procedure would benefit from robotic assistance to partially or fully automate this critical component of the intervention. A key component of automated kidney access, using a robotic manipulator, is to define and follow a tool path planning based on preoperative imaging and a target entry point.

In this paper, the use of the multiobjective non-dominated sorting genetic algorithm II (NSGA-II) is proposed to plan a B-spline curve that will be used as the tool trajectory during the procedure. Here, NSGA-II is used to determine the anchor point locations for a uniform 3rd order B-spline curve. The optimal path minimizes path length, tissue potential energy due to tissue compression, and path smoothness while maximizing the distance to obstacles. The multiobjective optimization is evaluated using simulations and physical trials. The results show that the planned trajectories show minimal tissue deformation, are relatively short and smooth and do not collide with the internal kidney structures.

## I. INTRODUCTION

Percutaneous Nephrolithotomy (PCNL) is the leading treatment for large or irregularly shaped kidney stones. This procedure aims to remove kidney stones by making a small incision in the patient's back through which narrow tools are threaded to reach the calculi [1], [2]. The most critical aspect of this procedure is gaining proper access to the kidney stones [3]. Despite the procedure's clinical prevalence for decades, only 11% of urologists gain kidney access themselves [4]. It is estimated that urologists require roughly 36 to 60 procedures to gain proficiency [5].

During PCNL, a tool must enter through the incision made in the patient's back and continues at a slight angle towards the kidney such that the tool enters the kidney in the correct location. Once inside the kidney, the tool must be steered towards the areas affected by kidney stones.

Inadequate tool steering leads to a higher chance of complications and increased recovery times due to additional injuries that may be suffered as a result of tissue damage.

We acknowledge the support of Marion Surgical and the Natural Sciences and Engineering Research Council of Canada (NSERC), [funding reference number 2018-06074].

Cette recherche a été menée en collaboration avec Marion Surgical et a été financée par le Conseil de recherches en sciences naturelles et en génie du Canada (CRSNG), [numéro de référence 2018-06074].

<sup>1</sup>O. Wilz (corresponding author), and C. Rossa are with the Faculty of Engineering and Applied Science, Ontario Tech University, Oshawa, ON, Canada. E-mail: olivia.wilz@ontariotechu.ca; rossa@sce.carleton.ca.

<sup>2</sup>B. Sainsbury is with Marion Surgical, Toronto, On, Canada. E-mail: ben@marionsurgical.com

These complications, while not fatal, lead to longer recovery times and excessive bleeding [6], [7], [8], [9]. These issues make it clear that partially or fully automating kidney access through robotic assistance could improve the procedure success rates and increase patient safety [10], [11], [12]. Automation of a sub-task during surgery allows the surgeon to take on a more supervisory role during the procedure and shifts much of the workload to procedure preparation, such as preoperative imaging and tool path planning.

Path planning is integral to any automated surgical procedure. A carefully planned path allows the robot to perform its task effectively and precisely with minimal risks to the outcome of a procedure. There are a few common traits of a desirable path regardless of application, such as being relatively short, smooth, and avoiding obstacles. During PCNL specifically, the ideal path is the one that provides access to the kidney while avoiding surrounding tissue and other anatomical structures that are at risk of unnecessary puncture due to their proximity to the kidney. It is also desirable to reduce tissue damage, which can be quantified as reducing the overall tissue displacement for a planned trajectory. While the literature for path planning in robotic surgery is extensive, little research has been done for PCNL path planning. PCNL differs from some of these procedures specifically in the assumptions made during the planning process, such as the tool being rigid throughout the procedure, and the tool-tissue interaction mostly occurs along the entry path [5].

This paper proposes a novel multiobjective path planner for autonomous kidney stone access during PCNL. Multiobjective non-dominated sorting genetic algorithm II (NSGA-II) is proposed to plan a B-spline curve through a set of anchor points that represents the desired tooltip trajectory from the entry point to the stone location. The optimization process considers the affect of the entire tool on surrounding tissue. Outputs of the algorithm are the optimal spline coefficients that minimize path length, tissue potential energy, and path smoothness, and maximizes the distance to obstacles.

The paper is organized as follows. Section II provides a brief overview of documented path planning algorithms in robotic surgery and introduces the B-splines and NSGA-II optimizer. The multiobjective optimization is first evaluated through a set of simulations in Sec. III and demonstrates the effectiveness of the path planning for a variety of goal locations within the kidney. The simulation shows that the planned trajectories result in minimal tissue deformation, are relatively short and smooth, and do not collide with the internal kidney structures, while the tool poses are

feasible. Finally, the trajectories are put into practice through physical experiments to demonstrate their applicability, this is discussed further in Sec. IV. To the best of the author's knowledge, this is the first implementation of a multiobjective optimizer combining B-spline for robot-aided PCNL.

## II. PCNL OPTIMAL PATH PLANNING

A wide variety of path planning algorithms have been applied to path planning in robotic surgery. These algorithms include several classical methods as well as evolutionary approaches. Some approaches are designed for online path planning where only the tool's immediate surroundings and the desired goal location are required. These include artificial potential fields, collision cones, vector field histograms, and dynamic windows [13], [14]. Online path planners are computationally effective, however, they are best suited to local path planning problems since they do not necessarily return an optimal path, but rather a *feasible path* that is primarily concerned with obstacle avoidance. Other planning methods, such as roadmap and grid-based approaches, are rather used to describe the environment as a whole, including obstacles and collision-free paths, and are frequently used in conjunction with additional search methods such as  $A^*$  or an evolutionary approach to return an *ideal path* [13], [14].

Evolutionary approaches to path planning are fast and often computationally efficient. They include a wide variety of swarm optimizers such as particle swarm optimization, ant colony optimization, bacterial foraging, bee colony optimization, and several lesser known swarm algorithms [13], [14]. Alternatively, genetic algorithms, fuzzy logic, and neural networks can also be used for path planning.

Surgical path planning must take into account a variety of objectives, thus, a multiobjective optimizer is a natural choice for the task of planning an autonomous trajectory for PCNL. The algorithm must consider multiple objectives to plan an ideal path and provide not one but multiple paths that are safe and effective in reaching the kidney stones. A frequently used and highly effective multiobjective algorithm, NSGA-II is well-known for its computational efficiency and performance. For example, in [15], NSGA-II is used to optimize the path planning task for an unspecified autonomous robot, where the paths are represented using splines to provide smooth trajectories.

In multiobjective optimizers, a high number of optimization variables can increase the computational time significantly. Therefore, to limit the dimension and the complexity of the problem, it is preferable if only a few coordinates are necessary to define the paths. For example, in order to maintain a smooth trajectory, a curve can be interpolated based on anchor points created by NSGA-II. Alternatively, B-splines can be used to represent these curves using only a few anchor points.

### A. PCNL Trajectory B-spline Representation

B-splines are well-suited to obstacle avoidance path planning tasks as they are computationally efficient and able to provide smooth continuous trajectories. The number of

anchors used to generate a B-spline increases the number of curves used to generate it and can increase the complexity of the resulting curve. B-splines are a piece-wise polynomial function constructed from a set of basis functions given as

$$N_{i,j}(t) = \frac{t - t_i}{t_{i+j} - t_i} N_{i,j-1}(t) + \frac{t_{i+j+1} - t}{t_{i+j+1} - t_{i+1}} N_{i+1,j-1}(t) \quad (1)$$

where  $j = 1, 2, \dots, d$ , and  $d$  is the degree of the B-spline being constructed. The degree of the spline is calculated with  $d = m - n - 1$  for a set of  $n + 1$  control points and a knot vector  $\mathbf{t} \in \mathbb{R}^{1 \times m+1}$ . When  $j = 0$  the basis function takes the form of

$$N_{i,0} = \begin{cases} 1 & t_i \leq t \leq t_{i+1} \\ 0 & \text{otherwise} \end{cases} \quad (2)$$

where  $t_i$  is the  $i^{\text{th}}$  entry in the knot vector which must be a non-decreasing series and each  $t_i \in [0, 1]$ . The final curve is then calculated as

$$C(t) = \sum_{i=1}^n \mathbf{P}_i N_{i,d}(t), \quad (3)$$

where  $\mathbf{P}_i \in \mathbb{R}^D$  are the coordinates of control point  $i$  for the dimension  $D$ , and  $N_{i,d}(t)$  is the corresponding basis function.

Splines are also well-suited to be used within an optimizer, as a relatively complex curve requires only a few control points  $\mathbf{P}$  to define it, thus keeping the dimensionality of the problem low. The objective of the optimizer is therefore to determine the coordinates of a limited number of control points such that the path created by them optimizes for a set of pre-defined cost functions.

### B. Multiobjective control point optimizer

NSGA-II uses four objectives when planning the ideal path for PCNL:

**Path Length** is to be minimized. For a 2 dimensional scenario  $C(t)$  contains the piecewise equations  $x(t)$  and  $y(t)$  which describe the  $x$  and  $y$  coordinates along the curve. Thus the path length can be defined as

$$f_1 = \int_a^b \sqrt{1 + \left(\frac{y'}{x'}\right)^2} dx \quad (4)$$

where  $x' = \frac{dx}{dt}$ ,  $y' = \frac{dy}{dt}$  and  $a \in \mathbb{R}^D$  and  $b \in \mathbb{R}^D$  are the start and end points of the path respectively.

**Obstacle Distance** describes the distance between the tool shaft and obstacles through the entire path trajectory. Maximizing the distance to an obstacle is important to avoid collisions with obstacles and keep the surgical tool as far away as possible from sensitive tissue during the procedure. To this end, the patient anatomy can be discretized as a set of voxels or pixels depending on the dimension of the problem. The center of each voxel or pixel is stored in a matrix  $T \in \mathbb{R}^{D \times \kappa}$  where  $\kappa$  is the total number of points used to describe the obstacle space. The distance to obstacles along the path must be maximized. First the path  $C(t)$  is

resampled such that there is a discrete set of evenly spaced points describing the path, this is denoted  $C_R(j) \in \mathbb{R}^{D \times \ell}$  where  $\ell$  is the total number of points used to describe the re-sampled path. The total distance to closest obstacles along the path can now be quantified as

$$f_2 = \sum_{j=1}^{\ell} \min \|C_R(j) - T\|. \quad (5)$$

It may be beneficial to consider the distance of the entire tool to its surrounding obstacles, with the tool pose known for each point along  $C_R(j)$ , (5) must be calculated and summed for the entire tool shaft. Thus (5) becomes

$$f_2 = \sum_{z=0}^L \sum_{j=1}^{\ell} \min \|C_{RT}(j, z) - T\|, \quad (6)$$

where  $L$  is the total length of the tool and  $C_{RT}(j, z)$  is a point at a distance  $z$  along the the tool shaft for the  $j^{th}$  point along the resampled path  $C_R(j)$ ; and when  $z = L$   $C_{RT}(j, L) = C_R(j)$ .

**Path Smoothness** is to be minimized to ensure that the path is smooth and free from unnecessary jerk. The smoothness of the path further ensures patient safety by minimizing rapid changes in motion that could cause additional tissue damage. The smoothness is quantified by

$$f_3 = \int_a^b \frac{(Q(t)/dt)^2}{\sqrt{x'^2 + y'^2}} dt \quad (7)$$

where

$$Q(t) = \frac{|x'y'' - y'x''|}{(x'^2 + y'^2)^{3/2}}; \quad (8)$$

here  $x'' = \frac{d^2x}{dt^2}$  and  $y'' = \frac{d^2y}{dt^2}$  [16].

**Tissue Compression Energy** is a measure of how much energy is stored in the patient tissue due to its compression for the entire desired tool trajectory. During PCNL, it is assumed that the tissue compression occurs along the tool's entry point in the kidney only. The tissue compression energy for a single point along the trajectory is given as

$$U(d) = \frac{1}{2} K \int_{z_1}^{z_2} s(z)^2 dz, \quad (9)$$

where  $z_1$  and  $z_2$  are the entry and exit depths along the tool axis respectively and

$$s(d, z) = \begin{cases} (z \cos \theta + x_t - x_{OP}(z)) & \text{if } z_1 \leq z \leq z_2 \\ 0 & \text{otherwise,} \end{cases} \quad (10)$$

where  $z$  is the distance along the tool axis,  $x_t$  is the horizontal coordinate of the tool base (where it is attached to the robot end-effector),  $\theta$  is the angle of the tool, and  $x_{OP}(z)$  is an equation describing the original entry path into the kidney, see Fig. 1(a).

The optimization variables are the coordinates for the anchor points, these anchor points are used in addition to the goal point and three constant points used to define a straight entry trajectory when creating the B-spline. Moving forward,

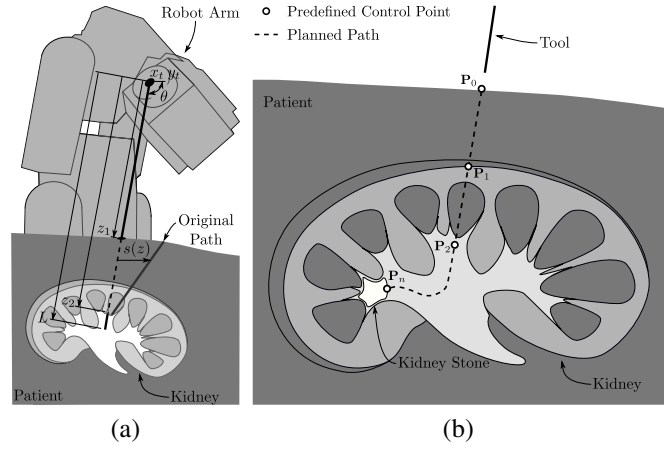


Fig. 1. Automated robotic PCNL overview, (a) shows a robot arm holding a nephroscope and how the tool enters the kidney, (b) shows 4 predefined constant control points and a possible B-spline created between these points leading to the kidney stone.

the anchor points created by the optimization algorithm may be referred to as the internal anchors. If five internal anchors are used in a 2-dimensional scenario, there is a total of 10 optimization variables ( $D \times \text{number of internal anchors}$ ).

A curve is generated for each of these population members and is then evaluated on the four cost functions described above. The evaluation of the cost functions requires that the tool pose is known. During autonomous PCNL kidney access, the tool is attached to the robot arm at its end-effector and the robot steers the tool from outside the tissue such that the tip follows the path to the end, that is, the location of the calculi. The inverse kinematics is presented in [10]. This is simulated during NSGA-II in order to evaluate the cost functions for every iteration along the discretized path.

The results of the cost functions determine the performance of each individual and affect the chance of a population member being used to generate the child population for the next iteration of the algorithm. The initial population is randomly generated, while each subsequent iteration of NSGA-II applies crossover and mutation schemes to the previous population to generate a new one. NSGA-II iterates until a stopping criterion is reached, in this case, a specified number of iterations. Once NSGA-II reaches the desired number of iterations, it returns the final population, the size of the final population is the same as that of the initial population or smaller, because the algorithm rejects solutions from the final set if they are not considered Pareto optimal.

### III. SIMULATION RESULTS

The proposed path planning method is first evaluated through a set of simulations. The simulations are performed for a simplified 2D version of the kidney and its anatomy, based on the phantom kidney used for the physical experiments in a later section, see Fig. 5. Additionally, three different goal points are considered, each goal is selected to demonstrate the algorithms ability to consider the surrounding environment; to this end **Goal 1** is located on the

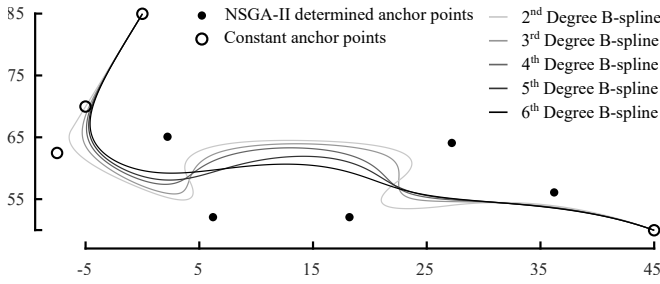


Fig. 2. Example of a B-spline with a total of 9 anchor points, constant anchor points are shown with circles, the first 3 ensure a relatively straight entry trajectory, the last one represents the goal point. The location of the internal anchors are determined by the NSGA-II algorithm (black dots). The degree of splines are depicted for 2<sup>nd</sup> to 6<sup>th</sup> degree splines ranging in color from light grey to dark grey respectively.

TABLE I  
NSGA-II ALGORITHM PARAMETERS

Simulation parameters		Workspace [mm]	
Dimension	10	$x$ range	$y$ range
Iterations	500		
Number of Objectives	4	min -60	min 40
Population Size	60	max 60	max 80

bottom left of the simulated anatomy, **Goal 2** is located on the bottom right, and **Goal 3** is located on the top left as shown in Fig. 3.

In scenarios 1 to 3, different end goals are specified. The only obstacles present in the kidney are considered to be the kidney walls. Hence, the tooltip is free to move inside of the kidney. One simulation is performed with an additional obstacle present in the environment, this is performed with Goal 1. These simulations are performed on an *Intel i7* processor with 64 GB of RAM and *GeForce RTX 2080* GPU.

During PCNL, the trajectory into the kidney is a straight path from the incision to where it enters a calyx. To ensure this entry trajectory remains straight and that the trajectory within the kidney is smooth and continuous along this first part of the trajectory, the first three control points for the B-spline are constant and determined in advance based on the desired entry trajectory. The final point for the uniform B-spline, or the goal point for the path, is also maintained as a constant for all of the B-splines. The NSGA-II algorithm controls the coordinates for five points between the three points defining a straight entry path and the final goal point see Fig. 2. For the 2D scenario described above, there will be a total of 10 variables that NSGA-II controls.

The simulation parameters are found in Table I; note that the population and number of iterations are kept relatively small compared to other optimization scenarios to reduce the computation time of the algorithm.

The results from the NSGA-II optimization for each simulation scenario can be seen in Fig. 3. In subfigure (a) is an example of a random initial population. Subfigures (b) to (d) show the final Pareto optimal solutions for each goal point. As it can be seen, the Pareto optimal solutions are all smooth curves that are relatively short and do not collide

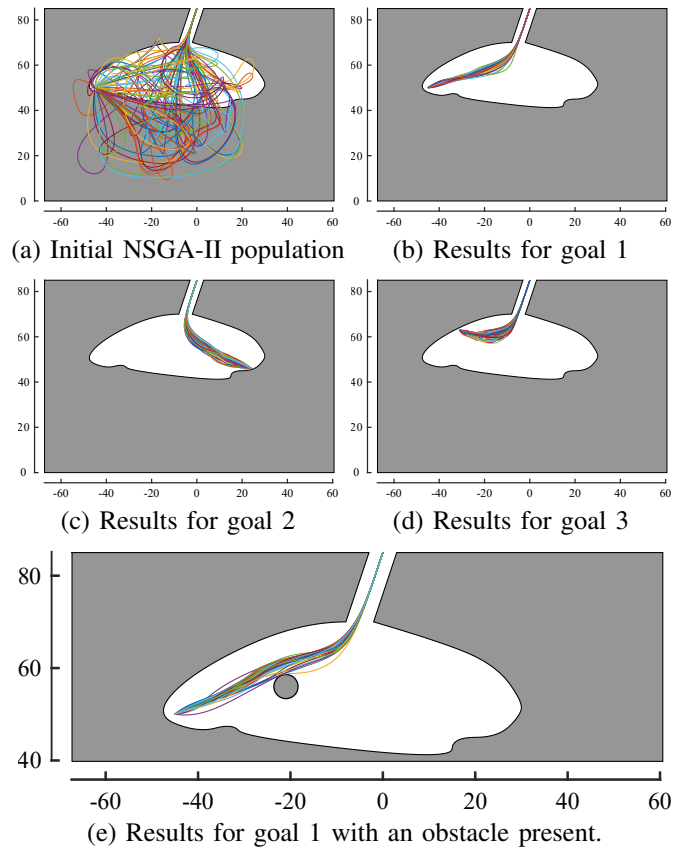


Fig. 3. The results from NSGA-II path planning, (a) shows an example of a randomly initialized population, (b)–(d) are the Pareto optimal solution sets returned for scenarios 1 through 3, (e) shows the Pareto optimal solutions for scenario 4 i.e. when an obstacle is present in the environment.

with any obstacles. Subfigure (e) shows the Pareto optimal solution for scenario 4, i.e., goal 1 when an obstacle is present, demonstrating the algorithm’s ability to create paths that still navigate around more complex surroundings with smooth trajectories.

From the Pareto optimal solution set, one member must be chosen to execute the task. This is a benefit of using a multi-objective optimizer that returns multiple solutions as it keeps a human in the loop of the planning procedure. Since all of the cost function values have been optimized to some degree, the generated solutions all represent acceptable trajectories. From these solutions, the operator can discard paths that are closer to obstacles than others, apply a maximum acceptable threshold to tissue compression, etc.

The cost function values are normalized relative to their respective minimums and maximums to compare them more easily. Furthermore, three out of the four cost functions must be minimized. For consistency, obstacle distance is inverted after normalization, thus in table II, lower values of obstacle distance are more desirable.

Selecting the optimal path from the Pareto front is then achieved in two steps. First, a subset of the final Pareto optimal solutions is selected. This is shown in Table II for scenario 3. The subset is selected by applying an upper

TABLE II

SUBSET OF THE NORMALIZED COST FUNCTION VALUES FOR SCENARIO 3

Member	Path length	Tissue energy	Path smoothness	Obstacle distance
4	0.2488	0.1471	$3.130 \times 10^{-10}$	0.4201
7	0.6501	0.0394	$9.563 \times 10^{-9}$	0.0441
8	0.3784	0.3950	$1.987 \times 10^{-12}$	0.5035
9	0.5804	0.2587	$4.951 \times 10^{-12}$	0.3939
11	0.1045	0.3088	1	0.3995
15	0.4690	0.2867	$1.458 \times 10^{-11}$	0.1650
22	0.7817	0.4025	0	0.2561
30	1	0	$5.681 \times 10^{-12}$	0
32	0.8116	0.3601	$1.299 \times 10^{-11}$	0.0004
46	0.6750	0.4377	$1.464 \times 10^{-13}$	0.6152

threshold of 0.65 and 0.72 to the normalized tissue energy and obstacle distance cost functions, respectively. Following this, the cost function values for each member are compared and members whose cost function values are too similar to a previous member are discarded. Cost function similarity is determined by the root-mean-squared of the difference between two members' fitness values.

In the second step, a single solution is then selected from the subset by inspecting each individual solution path visually, and by analyzing their cost function values. Since all paths tend to be relatively short, the other three cost functions may be given more weight during the decision. Obstacle distance is given priority.

The selected result for scenario 3 has been highlighted in light grey in Table II (member 32). This path is being selected since it has the second-lowest obstacle distance and shows good results in the other cost function values. Although member 32's highest value is the length of this path, this value is not the longest path generated across all Pareto solutions. This indicates a good trade-off between cost functions.

The resultant tool poses required to follow each of the optimal tooltip paths from each scenario are presented in Fig. 4. The tool poses determine the tissue compression during the NSGA-II, they are also used to perform the physical experiments described in the next section. From the simulation results, both the tooltip and the tool shaft do not intersect with the simulated obstacles. It is also worth noting that even though the tool shaft is not constrained to the entry point in the tissue, the optimal path keeps the tool shaft close to its entry point to avoid tissue damage.

#### IV. EXPERIMENTAL EVALUATION

The path planning algorithm is also validated through physical trials. The paths selected during simulations are executed using a 6-DOF robotic arm (Meca 500, Mecademic, Montréal, Canada) in a kidney phantom. The tool used in the physical experiments is a 218.7 mm long square brass rod with a width of 3.2 mm. An electromagnetic tool tracking system (Aurora, Northern Digital, Waterloo, Canada) records the tool's tip during the trials, see Fig. 5. The robot arm steers the tool base such that its tip follows the desired path. The robot's inverse kinematic is presented in detail in [10].

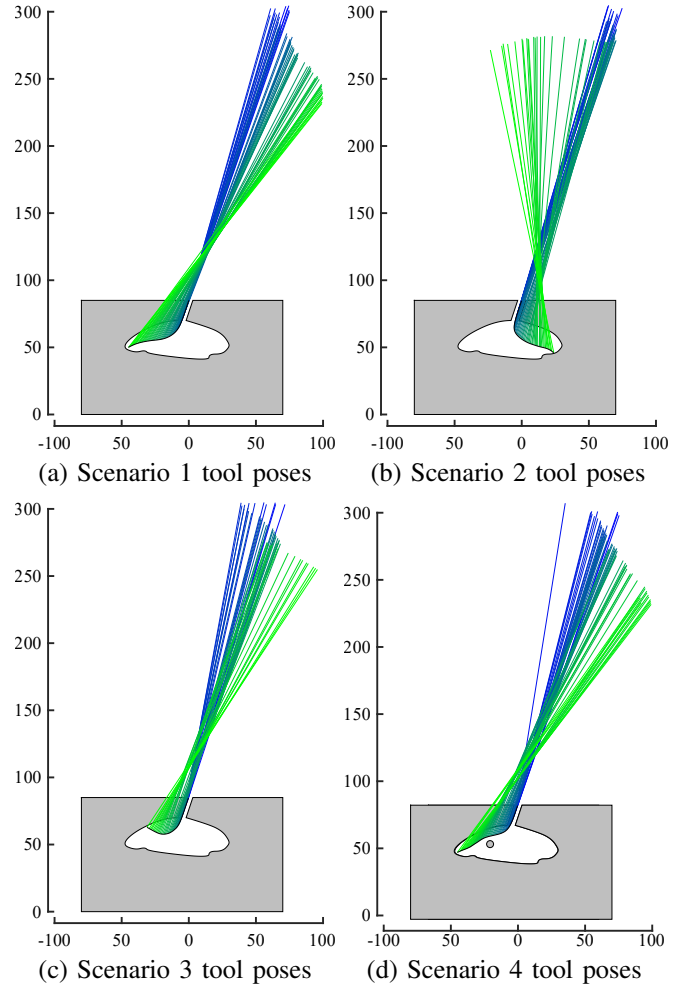


Fig. 4. The results of the path planning algorithm, an ideal path is selected for each scenario and plotted in (a)–(d) above along with the tool poses generated during the path planning process in order to reduce tissue compression. The tool poses are shown in blue at their starts and become green as they approach the goal point.

Each of the selected paths from the previous section is executed on this experimental setup to ensure that the paths are feasible. Each path is run three times. The recorded tooltip trajectory for each run is shown along with the reference trajectory in Fig. 6. While the obstacle is shown in the figure, note that it is not present in the phantom kidney and is only considered during the planning of scenario 4.

All paths follow their reference trajectories, entering the kidney on a straight line, thanks to the first 3 anchor points, and then following a curved line around the obstacle towards the goal. Both the tooltip and the tool shaft successfully avoid the obstacle and the kidney walls and the tooltip reaches the desired goal. Lateral tool motion is also minimized by the algorithm to limit tissue compression. The increased tracking error as the tool approaches the goal is the outcome of the assumption that the tool is perfectly rigid, which is not the case for the brass tool used in the experiments. Additionally, some error may be caused by electromagnetic interference in the tracking process.

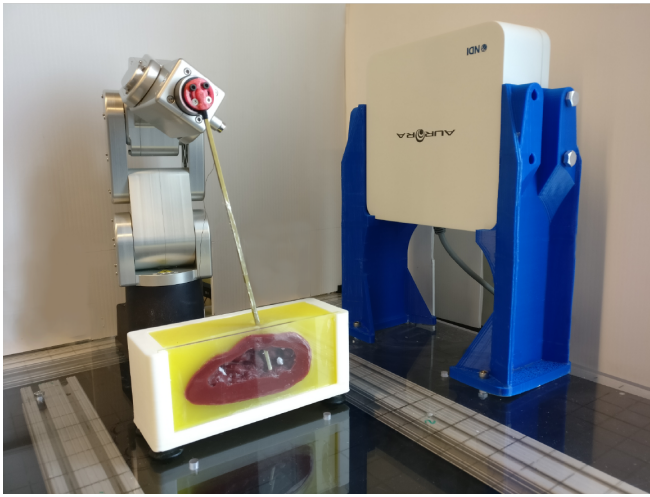


Fig. 5. Experimental setup used to conduct the experiments on a phantom kidney model. A brass rod is used as the nephroscope. The 6-degree-of-freedom robot steers the tool base such that the tooltip follows the predefined trajectory. The tooltip location is recorded by the electromagnetic tracking system.

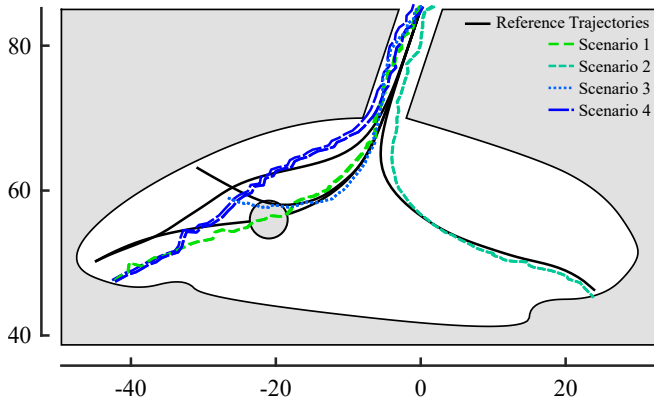


Fig. 6. Each of the selected paths are plotted along with the tooltip tracking results from the physical experimental trials. Scenario 4 (the dark blue path) is the only trajectory that needs to maneuver around the obstacle.

## V. CONCLUSION

Autonomous kidney access is an important component of both semi and fully autonomous versions of PCNL. To this end, this paper proposes a path planning framework for PCNL using B-spline representation with the multiobjective optimizer NSGA-II. The resulting trajectories meet several requirements: being short and smooth while avoiding obstacles and high tissue compression. The path planning algorithm is validated on four scenarios, demonstrating its ability to plan an appropriate trajectory given different circumstances. A single trajectory is selected from the Pareto optimal solution set that is returned by the algorithm, this selection process keeps a human in the loop of planning the procedure to further ensure patient safety. Each of the selected trajectories is evaluated with three physical trials, where a robot arm controls the tool and advances it along the planned path towards the goal. The physical trials demonstrate the ability of the system to avoid obstacles while

minimizing tissue damage at the entry point.

Future work will explore incorporating a tool bending model and a finite element model of the kidney tissue to better represent the coupled tool/tissue interaction. Furthermore, active feedback control using ultrasound images as position feedback will be investigated to enable real-time path planning for increased accuracy.

## REFERENCES

- [1] Thomas Knoll, Francisco Daels, Janak Desai, Andras Hoznek, Bodo Knudsen, Emanuele Montanari, Cesare Scoffone, Andreas Skolarikos, and Keiichi Tozawa, "Percutaneous nephrolithotomy: technique," *World Journal of Urology*, vol. 35, no. 9, pp. 1361–1368, 2017.
- [2] Jean J.M.C.H de La Rosette, Maria P Laguna, Jens J Rassweiler, and Pierre Conort, "Training in percutaneous nephrolithotomy—a critical review," *European Urology*, vol. 54, no. 5, pp. 994–1003, 2008.
- [3] Federica Ferraguti, Marco Minelli, Saverio Farsoni, Stefano Bazzani, Marcello Bonfè, Alexandre Vandanjon, Stefano Puliatti, Giampaolo Bianchi, and Cristian Secchi, "Augmented reality and robotic-assistance for percutaneous nephrolithotomy," *IEEE Robotics and Automation Letters*, vol. 5, no. 3, pp. 4556–4563, 2020.
- [4] Vincent G Bird, Bernard Fallon, and Howard N Winfield, "Practice patterns in the treatment of large renal stones," *Journal of endourology*, vol. 17, no. 6, pp. 355–363, 2003.
- [5] B. Sainsbury, M. Lacki, M. Shahait, M. Goldenberg, A. Baghdadi, L. Cavuoto, J. Ren, M. Green, J. Lee, T. D'Averch, , and C. Rossa, "Evaluation of a virtual reality percutaneous nephrolithotomy (pcnl) surgical simulator," *Frontiers in Robotics and AI*, vol. 6:145, 2020.
- [6] Iason Kyriazis, Vasilios Panagopoulos, Panagiotis Kallidonis, Mehmet Ozsoy, Marinos Vasilas, and Evangelos Liatsikos, "Complications in percutaneous nephrolithotomy.(report)," *World Journal of Urology*, vol. 33, no. 8, pp. 1069–1077, 2015-08-01.
- [7] Maurice Stephan Michel, Lutz Trojan, Jens Jochen Rassweiler, and Alberto Breda, "Complications in percutaneous nephrolithotomy," *European Urology*, vol. 51, no. 4, pp. 899,906, 2007-04.
- [8] Soroush Rais-Bahrami, Justin I. Friedlander, Brian D. Duty, Zeph Okeke, and Arthur D. Smith, "Difficulties with access in percutaneous renal surgery," *Therapeutic Advances in Urology*, vol. 3, no. 2, pp. 59–68, 2011.
- [9] Carissa Chu, Selma Masic, Manint Usawachintachit, Weiguo Hu, Wenzeng Yang, Marshall Stoller, Jianxing Li, and Thomas Chi, "Ultrasound-guided renal access for percutaneous nephrolithotomy: A description of three novel ultrasound-guided needle techniques," *Journal of Endourology*, vol. 30, 09 2015.
- [10] O. Wilz, B. Sainsbury, and C. Rossa, "Constrained haptic-guided shared control for collaborative human-robot percutaneous nephrolithotomy training," *Mechatronics*, vol. 75, pp. 102528, 2021.
- [11] Li-Ming Su, Dan Stoianovici, Thomas W Jarrett, Alexandru Patriciu, William W Roberts, Jeffrey A Cadeddu, Sanjay Ramakumar, Stephen B Solomon, and Louis R Kavoussi, "Robotic percutaneous access to the kidney: comparison with standard manual access," *Journal of Endourology*, vol. 16, no. 7, pp. 471–475, 2002.
- [12] Ben Challacombe, Alexandru Patriciu, Jonathan Glass, Monish Aron, Tom Jarrett, Fernando Kim, Peter Pinto, Dan Stoianovici, Nigel Smeeton, Richard Tiptaft, et al., "A randomized controlled trial of human versus robotic and telerobotic access to the kidney as the first step in percutaneous nephrolithotomy," *Computer aided surgery*, vol. 10, no. 3, pp. 165–171, 2005.
- [13] Purushothaman Raja and Sivagurunathan Pugazhenthii, "Optimal path planning of mobile robots: A review," *International journal of physical sciences*, vol. 7, no. 9, pp. 1314–1320, 2012.
- [14] Mohd Nayab Zafar and JC Mohanta, "Methodology for path planning and optimization of mobile robots: A review," *Procedia computer science*, vol. 133, pp. 141–152, 2018.
- [15] F Ahmed and Kalyanmoy Deb, "Multi-objective path planning using spline representation," in *2011 IEEE International Conference on Robotics and Biomimetics*. 2011, pp. 1047–1052, IEEE.
- [16] T Berglund, A Brodnik, H Jonsson, M Staffanson, and I Soderkvist, "Planning smooth and obstacle-avoiding b-spline paths for autonomous mining vehicles," *IEEE transactions on automation science and engineering*, vol. 7, no. 1, pp. 167–172, 2010.